Title
Formin-dependent TGF-β signaling for epithelial to mesenchymal transition.

Journal
Molecular biology of the cell, 29(12)

ISSN
1059-1524

Authors
Rana, Manish K
Aloisio, Francesca M
Choi, Changhoon
et al.

Publication Date
2018-06-01

DOI
10.1091/mbc.e17-05-0325

Peer reviewed

Formin-dependent TGF-β signaling for epithelial to mesenchymal transition

Manish K. Rana[a], Francesca M. Aloisio[a], Changhoon Choi[b], and Diane L. Barber[a,*]
[a]Department of Cell and Tissue Biology, University of California, San Francisco, San Francisco, CA 94143;
[b]Department of Radiation Oncology, Samsung Medical Center, Seoul 06351, South Korea

ABSTRACT **The role of distinct actin filament architectures in epithelial plasticity remains incompletely understood. We therefore determined roles for formins and the Arp2/3 complex, which are actin nucleators generating unbranched and branched actin filaments, respectively, in the process of epithelial to mesenchymal transition (EMT). In clonal lung, mammary, and renal epithelial cells, the formin activity inhibitor SMIFH2 but not the Arp2/3 complex activity inhibitor CK666 blocked EMT induced by TGF-β. SMIFH2 prevented the proximal signal of increased Smad2 phosphorylation and hence also blocked downstream EMT markers, including actin filament remodeling, decreased expression of the adherens junction protein E-cadherin, and increased expression of the matrix protein fibronectin and the transcription factor Snail. The short hairpin RNA silencing of formins DIAPH1 and DIAPH3 but not other formins phenocopied SMIFH2 effects and inhibited Smad2 phosphorylation and changes in Snail and cadherin expression. Formin activity was not necessary for the cell surface expression or dimerization of TGF-β receptors, or for nuclear translocation of TAZ, a transcription cofactor in Hippo signaling also regulated by TGF-β. Our findings reveal a previously unrecognized role for formin-dependent actin architectures in proximal TGF-β signaling that is necessary for Smad2 phosphorylation but not for cross-talk to TAZ.**

Monitoring Editor
Margaret Gardel
University of Chicago

Received: May 26, 2017
Revised: Apr 5, 2018
Accepted: Apr 10, 2018

INTRODUCTION

The process of epithelial to mesenchymal transition (EMT) is critical for normal development and tissue remodeling and contributes to the progression of diseases such as fibrosis and cancer metastasis (Kalluri and Neilson, 2003; Kalluri and Weinberg, 2009; Borok *et al.*, 2011). EMT is often considered as two complementary programs, one morphological and another transcriptional. The morphological program includes acquiring a mesenchymal cell shape and remodeling of actin filaments from a cortical ring in epithelial cells to abundant ventral stress fibers. The transcriptional program includes decreased expression of the adherens junction protein E-cadherin, which disrupts cell–cell contacts and enables a mesenchymal morphology, and increased production of the extracellular matrix proteins fibronectin and collagen, which when dysregulated contributes to fibrosis (Xu *et al.*, 2009). Although the transcriptional program for EMT is well characterized and known to be coordinated primarily through activation of transcription factors in the Snail, ZEB, and Twist families that repress expression of epithelial genes and activate expression of mesenchymal genes (Xu *et al.*, 2009), we know less about how the morphological program of EMT is controlled and whether it also regulates transcriptional events.

In most EMT models, the morphological program requires activity of the low-molecular-weight GTPase RhoA and RhoA-kinase (ROCK) (Bhowmick *et al.*, 2001; Tavares *et al.*, 2006; Cho and Yoo, 2007). In selective cell models, cytoskeleton remodeling during EMT also depends on changes in the expression of actin regulatory proteins, such as moesin (Haynes *et al.*, 2011), zyxin (Mori *et al.*, 2009), and the formins FHOD1 (Jurmeister *et al.*, 2012) and FMNL2

This article was published online ahead of print in MBoC in Press (http://www.molbiolcell.org/cgi/doi/10.1091/mbc.E17-05-0325) on April 18, 2018.

*Address correspondence to: Diane L. Barber (diane.barber@ucsf.edu).

Abbreviations used: DAAM1, disheveled-associated activator of morphogenesis 1; DAAM2, disheveled-associated activator of morphogenesis 2; DIAPH1, protein diaphanous homologue 1; DIAPH2, protein diaphanous homologue 2; DIAPH3, protein diaphanous homologue 3; EMT, epithelial to mesenchymal transition; FHOD1, FH1/FH2 domain-containing protein 1; FMNL1, formin-like protein 1; FMNL2, formin-like protein 2; MRTF, myocardin-related transcription factor; p-MLC, phosphorylated myosin light chain; pSmad2, phosphorylated Smad2; SRF, serum response factor; TGF-β, transforming growth factor-β; TGF-βR1, TGF-β receptor type 1; TGF-βR2, TGF-β receptor type 2.

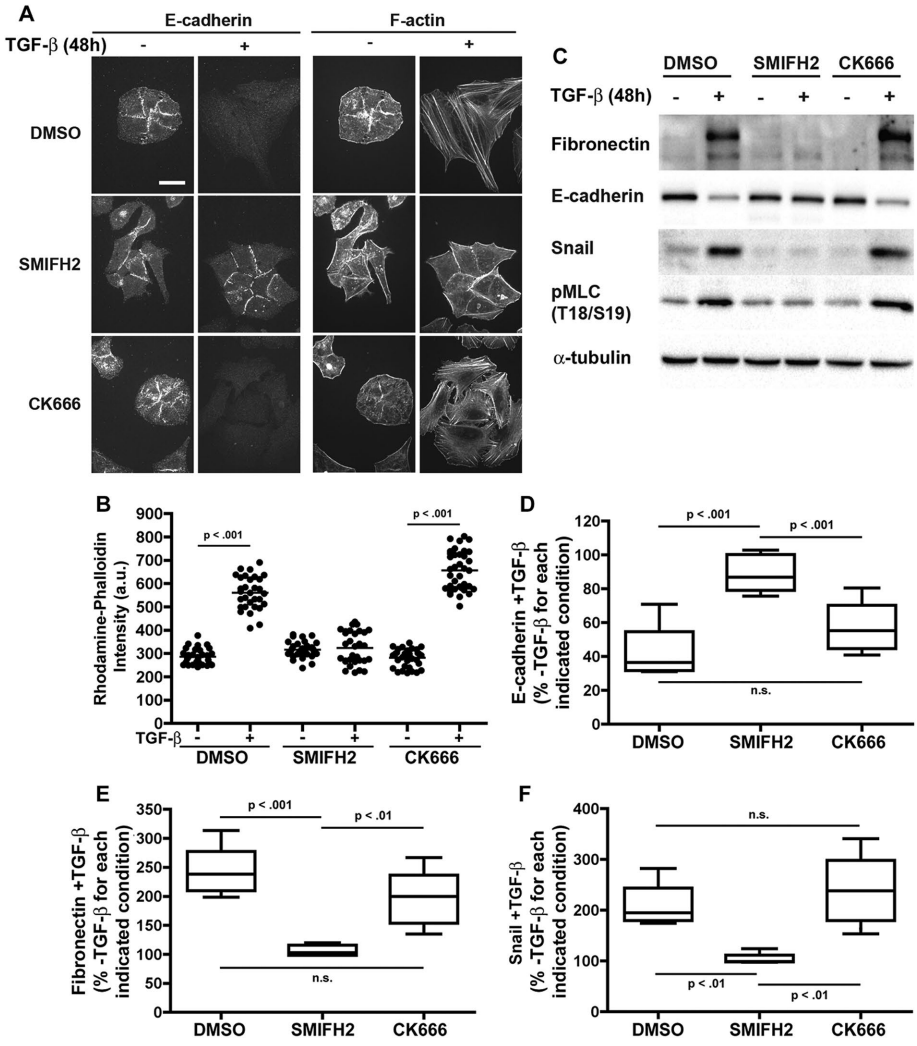

FIGURE 1: The formin inhibitor SMIFH2 but not the Arp2/3 complex inhibitor CK666 blocks EMT of A549 cells with TGF-β. (A) Images of A549 cells maintained in the absence (–) or presence (+) of TGF-β for 48 h without (DMSO control) or with SMIFH2 or CK666 immunolabeled for E-cadherin and stained for F-actin with rhodamine–phalloidin. Representative confocal images show mononchromatic LUT of maximum-intensity projections of multiple Z-sections. Bar, 20 μm. (B) Quantification of rhodamine–phalloidin intensity for the indicated conditions in the absence (–) or presence (+) of TGF-β for 48 h. Data were obtained from 30–35 cells per condition from three independent cell preparations. (C) Immunoblots of lysates from A549 cells maintained in the absence (–) or presence (+) of TGF-β for 48 h without (DMSO control) or with SMIFH2 or CK666 probed with antibodies to fibronectin (FN), E-cadherin, Snail, phosphorylated MLC (pMLC), and α-tubulin (loading control). (D–F) Semiquantitative densitometry of immunoblots described in C probed for E-cadherin (D), fibronectin (E), and Snail (F). Boxes show the median ± 95% confidence intervals with whiskers indicating smallest and largest values. Statistical analysis by two-tailed *t* test of six cell preparations for E-caherin, five for fibroectin, and four for Snail.

(Li *et al.*, 2010). However, these regulators of the EMT morphological program are generally not necessary for transcriptional events with EMT.

In the current study we investigated roles for two distinct actin nucleators in EMT, in part to resolve how distinct actin architectures regulate epithelial plasticity and in part to test whether actin regulators contribute to the transcriptional program of EMT.

We found that activity of formins, which nucleates the assembly of unbranched actin filaments (Goode and Eck, 2007; Schonichen and Geyer, 2010) but not activity of the Arp2/3 complex, which nucleates the assembly of branched actin filaments (Goley and Welch, 2006), is necessary for EMT of clonal lung, mammary, and renal epithelial cells induced by the cytokine transforming growth factor-beta (TGF-β). Inhibiting formins completely blocked both transcription and morphological effects, including suppressing expression of the transcription factor Snail and blocking decreased expression of E-cadherin as well as preventing actin filament remodeling to contractile stress fibers and a mesenchymal cell morphology. A role for formin activity in morphological and transcriptional events suggested it might be necessary for proximal TGF-β signaling, which we confirmed by showing that formin but not Arp2/3 complex activity is necessary for the initial TGF-β signaling event of increased phosphorylation of Smad2 (pSmad2 S465/467) and the subsequent nuclear translocation of Smad2. Using short hairpin RNA (shRNA) for selective formin family members, we found that DIAPH1 and 3 are necessary for increased pSmad2 and Snail as well as actin filament remodeling, indicating a role in both transcriptional and morphological programs. These findings have broad significance for a mechanistic understanding of the many cell behaviors regulated by TGF-β and requiring EMT.

RESULTS

Formin but not Arp2/3 complex activity is necessary for EMT

We first tested the importance of actin nucleators for EMT of human lung alveolar A549 cells by using well-characterized and selective pharmacological inhibitors of formin and Arp2/3 complex activity. We treated cells with TGF-β for 48 h, which induces EMT in diverse epithelial cell types (Heldin and Moustakas, 2012), in the absence and presence of the broad-spectrum formin inhibitor SMIFH2 that targets the conserved FH2 domain in all 15 mammalian formins (Rizvi *et al.*, 2009; Ganguly *et al.*, 2015) and the Arp2/3 complex inhibitor CK666 that stabilizes the inactive conformation of the complex by allosterically blocking conformational changes in subunits (Nolen *et al.*, 2009; Yang *et al.*, 2012). Consistent with previous reports on EMT of A549 cells with TGF-β (Xi *et al.*, 2014; Rana *et al.*, 2015), control cells in the absence of inhibitors had decreased expression of E-cadherin (Figure 1, A, C, and D), remodeling of actin filaments from a cortical ring in epithelial cells to abundant parallel ventral stress fibers traversing the mesenchymal cell body (Figure 1, A and B), and increased expression of the extracellular matrix protein fibronectin (Figure 1, C and E) and the transcription factor Snail (Figure 1, D and F). Control cells also had an increase in phosphorylated myosin light chain (pMLC; pT18/pS19) (Figure 1C), consistent with transition to a mesenchymal contractile phenotype.

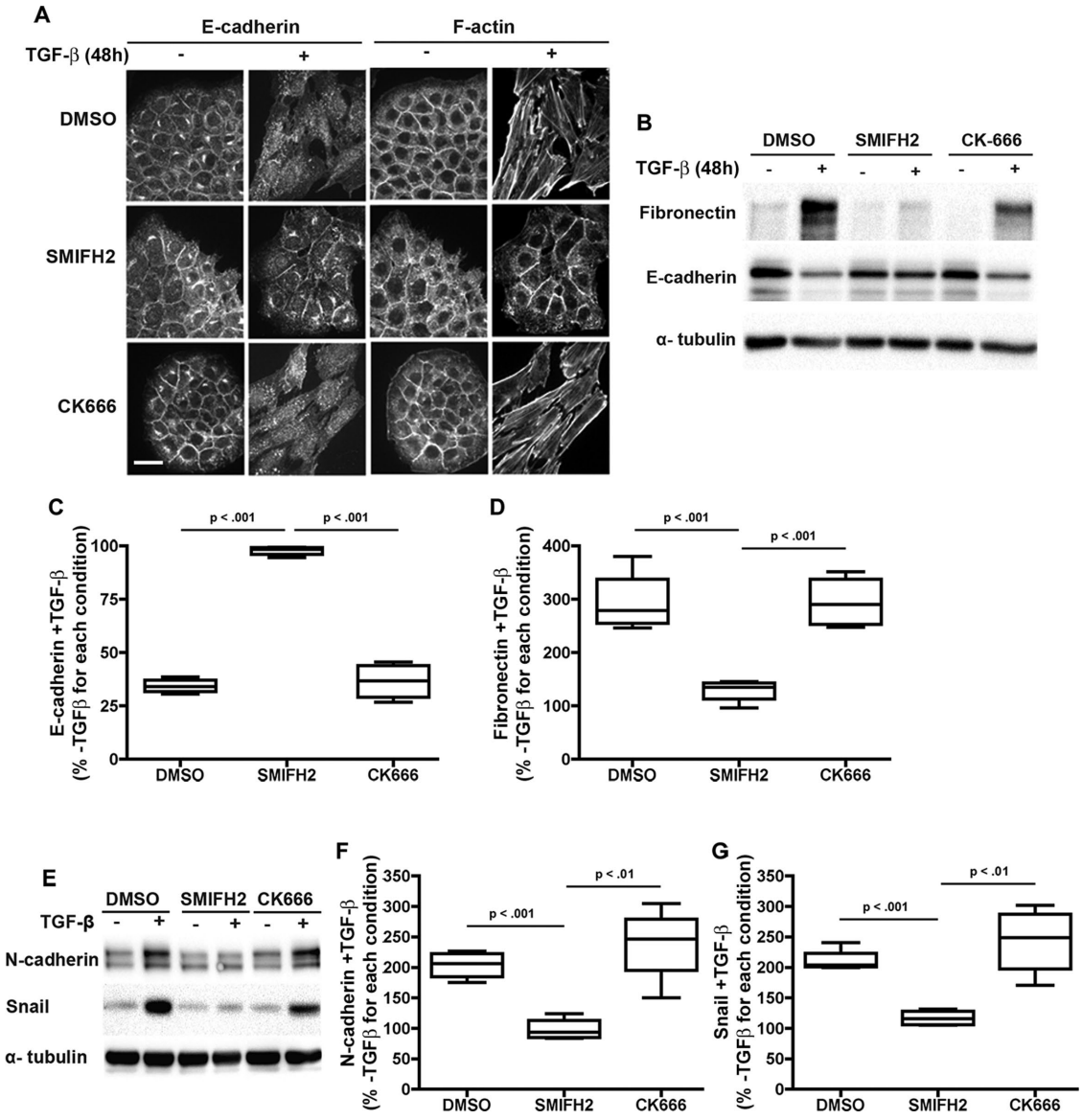

FIGURE 2: SMIFH2 but not CK666 blocks EMT of NMuMG and HK2 cells with TGF-β. (A–D) NMuMG cells maintained in the absence (–) or presence (+) of TGF-β without and with SMIFH2 or CK666 for 48 h were immunolabeled for E-cadherin and stained for F-actin with rhodamine–phalloidin (A) (bar, 20 μm) and lysates immunoblotted for E-cadherin, fibronectin, and α-tubulin (B). Semiquantitative densitometry of immunoblots described in B probed for E-cadherin (C); fibronectin (D) determined from four separate cell preparations. (E–G) Lysates of HK2 cells maintained as described for NMuMG cells immunoblotted for N-cadherin (E, F) and Snail (E, G) with semiquantitative densitometry determined from four separate cell preparations. In C, D, F, and G, boxes show the median ± 95% confidence intervals with whiskers indicating smallest and largest values.

All of these changes with EMT of A549 cells were suppressed by the formin inhibitor SMIFH2 but not by the Arp2/3 complex inhibitor CK666 (Figure 1, A–F). To confirm the efficacy of CK666 and specificity of SMFH2, we tested their effects on the velocity of *Listeria monocytogenes* in mammalian host cells. *Listeria* motility is dependent on host-cell actin filament assembly generated by the Arp2/3 complex (Welch *et al.*, 1997; May *et al.*, 1999). We found that CK666 but not SMIFH2 significantly decreased *Listeria* velocity (Supplemental Figure S1).

We also confirmed that SMIFH2 but not CK666 blocked EMT induced by TGF-β in two additional well-characterized clonal cells models, NMuMG mouse mammary epithelial cells (Miettinen *et al.*, 1994; Bhowmick *et al.*, 2001; Lamouille and Derynck, 2007; Haynes *et al.*, 2011), and HK2 human kidney epithelial cells (Jeon *et al.*, 2015; Rana *et al.*, 2015). EMT in NMuMG cells includes remodeling of actin filaments into stress fibers (Figure 2A), delocalization of E-cadherin from cell–cell contacts, and decreased E-cadherin expression (Figure 2, A–C) and increased fibronectin expression (Figure 2, B and D). Characteristics of EMT in HK2 cells include increased expression of N-cadherin and Snail (Figure 2, E–G). These well characterized markers of EMT in both cell types were significantly blocked by SMIFH2 but not CK666 (Figure 2, A–G), which with our data for A549 cells indicate that inhibiting activity of formins but not the Arp2/3 complex prevents both morphological and transcriptional programs of EMT in distinctly different types of epithelial cells.

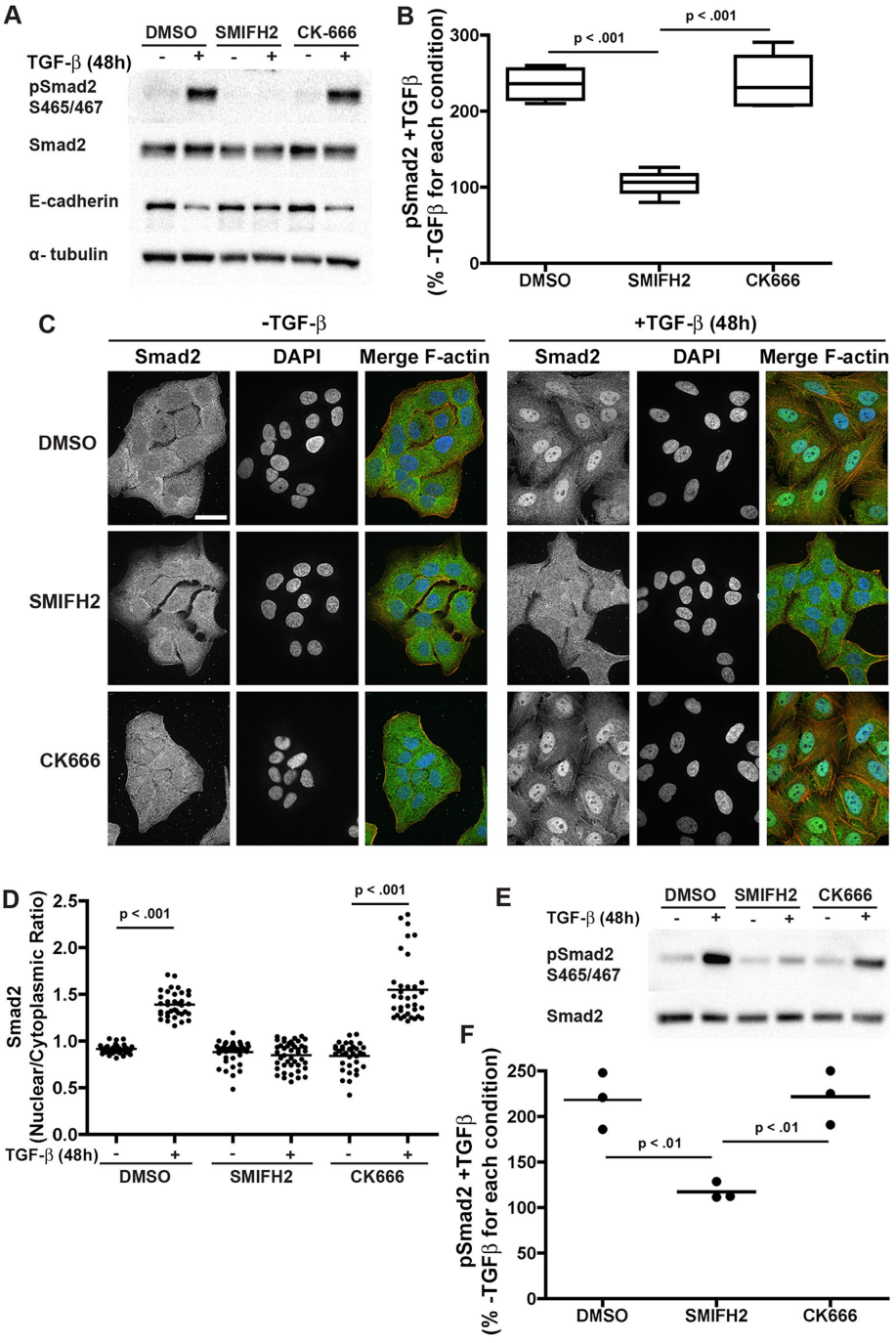

FIGURE 3: SMIFH2 but not CK666 blocks increased pSmad2 with TGF-β. (A) Immunoblots of lysates from A549 cells maintained for 48 h in the absence (–) or presence (+) of TGF-β for 48 h without (DMSO) or with SMIFH2 or CK666 probed for phosphorylated Smad2 (pSmad2), total Smad2, E-cadherin, and α-tubulin. (B) Semiquantitative densitometry of immunoblots probed for pSmad2 as shown in A from four independent cell preparations. Boxes show the median ± 95% confidence intervals with whiskers indicating smallest and largest values. (C) Confocal images of A549 cells maintained for 48 h in the absence (–) or presence (+) of TGF-β for 48 h without (DMSO) or with SMIFH2 or CK666 immunolabeled for Smad2 (green) and costained with DAPI for nuclei (blue) and rhodamine–phalloidin for actin filaments (magenta). Bar, 20 μm. (D) Nuclear to cytoplasmic ratio of Smad2 from immunolabeling as shown in C quantified for 36–48 cells per condition from three independent cell preparations. (E) Immunoblots of lysates from HK2 cells maintained in the absence (–) or presence (+) of TGF-β for 48 h without (DMSO) or with SMIFH2 or CK666 probed for pSmad2 and total Smad2. (F) Semiquantitative densitometry of pSmad2 immunoblots as shown in E from three independent cell preparations.

Formin activity is necessary for phosphorylation of Smad2 with TGF-β

The ability of SMIFH2 to block morphological and transcription changes with EMT suggested it might act at a proximal step in TGF-β signaling. Consistent with this prediction, we found that increased phosphorylation of Smad2 (S465/467; pSmad2) in A549 cells treated with TGF-β for 48 h was blocked by SMIFH2 but not CK666 (Figure 3, A and B). Total Smad2 was unchanged in the absence or presence of TGF-β or inhibitors. Phosphorylated Smad2, an initial effector of the activated TGF-β receptor, forms a complex with other Smad proteins and translocates to the nucleus to complex with transcription regulators repressing or activating target genes such as E-cadherin, Snail, and fibronectin (Heldin and Moustakas, 2012; Lamouille *et al.*, 2014). To score for nuclear Smad2 we immunolabeled A549 cells with antibodies to total Smad2 because available pSmad2 antibodies are not effective for immunolabeling and stained nuclei with 4′,6-diamidino-2-phenylindole (DAPI) and actin filaments with rhodamine-phalloidin. We confirmed an increase in the nuclear-to-cytoplasmic ratio of Smad2 after 48 h with TGF-β in dimethyl sulfoxide (DMSO) controls that was inhibited by SMIFH2 but not CK666 (Figure 3, C and D). The nuclear-to-cytoplasmic ratio of Smad2 in the absence of TGF-β was similar in control cells and cells treated with SMIFH2 or CK666 (Figure 3, C and D). We also confirmed an increase in pSmad2 in DMSO control HK2 cells treated with TGF-β for 48 h that was blocked by SMIFH2 but not CK66 (Figure 3 E and F). These data with two different EMT cell models, human lung alveolar A549 cells and kidney HK2 cells, indicate formin activity is necessary for the proximal TGF-β signaling event of increased pSmad2, which to our knowledge has not been previously reported.

To further test formin-dependent pSmad2, we determined acute (≤60 min) compared with longer-term (48 h) responses to TGF-β. In DMSO controls of A549 cells, pSmad2 increased between 10 and 60 min with TGF-β, determined by immunoblotting cell lysates (Figure 4, A and B). Additionally, immunolabeling for total Smad2 indicated increased nuclear localization at 60 min after adding TGF-β (Figure 4, C and D). Both of these responses were completely blocked by SMIFH2 (Figure 3, A–D), indicating a necessary role for formin activity in rapid as well as longer-term TGF-β signaling. However, when we added SMIFH2 30 min after ligand treatment, the abundance of

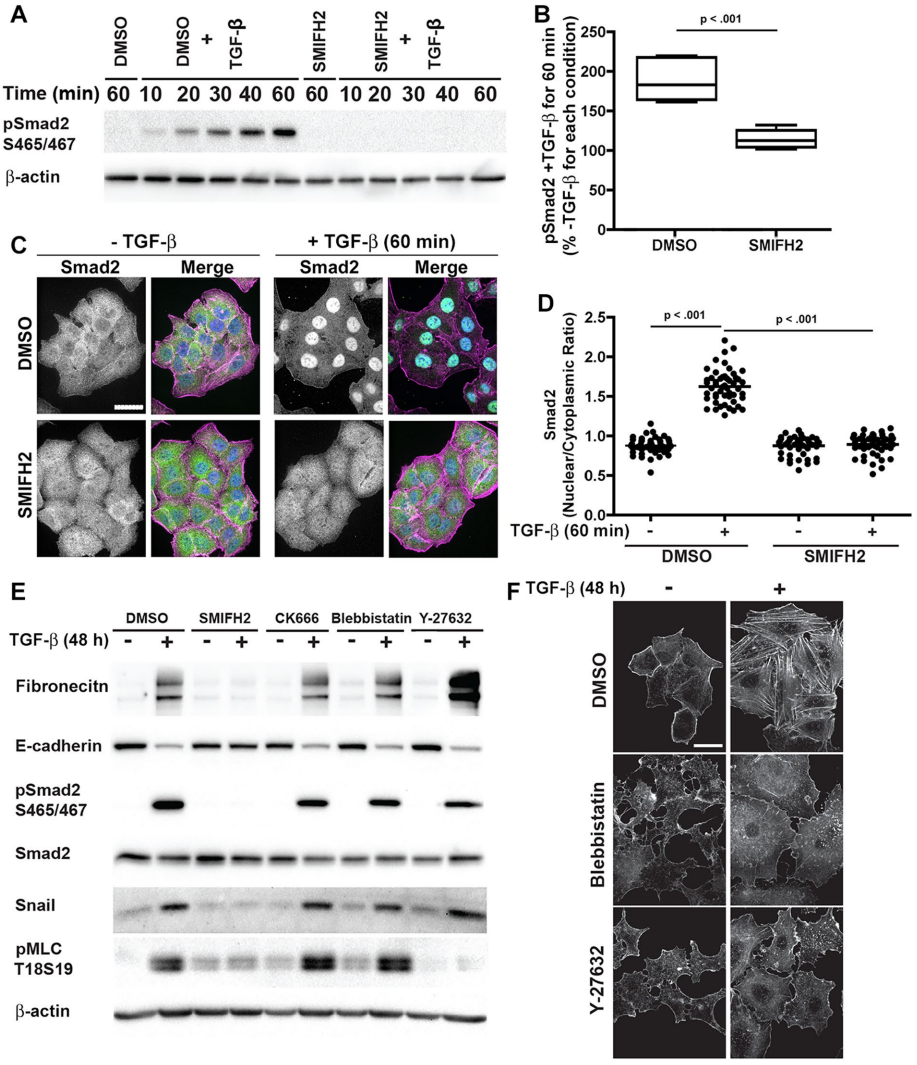

FIGURE 4: Inhibiting formin activity but not actomyosin contractility blocks increased pSmad2 with TGF-β. (A) Immunoblots of lysates from A549 cells maintained in the absence (–) or presence (+) of TGF-β without (DMSO control) or with SMIFH2 for the indicated times probed for pSmad2 and β-actin. (B) Semiquantitative densitometry of immunoblots for pSmad described in A at 60 min from five independent cell preparations. Boxes show the median ± 95% confidence intervals with whiskers indicating smallest and largest values. (C) Confocal images A549 cells immunolabeled for Smad2 (green) and costained with DAPI for nuclei (blue) and rhodamine–phalloidin for actin filaments (magenta). Bar, 20 μm. (D) Nuclear to cytoplasmic ratio of Smad2 from immunolabeling as shown in C. Data were obtained from 35 to 45 cells per condition from three independent cell preparations. (E) Immunoblots of lysates from A549 cells maintained in the absence (–) or presence (+) of TGF-β for 48 h without (DMSO) or with SMIFH2, CK666, Blebbistatin, or Y-27632 probed with for fibronectin, E-cadherin, pSmad2, total Smad2, Snail, pMLC, and β–actin. Data are representative of two independent cell preparations. (F) Confocal images of the A549 cells with the indicated treatments and stained with rhodamine–phalloidin to visualize actin filaments. Images show maximum-intensity projections of multiple Z-sections and are representative of two separate cell preparactions. Bar, 20 μm.

pSmad2 decreased to only 50% of DMSO controls, compared with being nearly abolished when the inhibitor was added at the same time as ligand (Supplemental Figure S2A). These findings suggest initial signaling to pSmad2 is fully dependent on formin activity but only partially dependent after the signal is initiated. Additionally, we confirmed that Smad2 phosphorylation and nuclear translocation are dependent on an intact actin cytoskeleton by treating cells with latrunculin, which binds G-actin and disrupts actin filament assemblies. Pretreating A549 cells with 5 μM latrunculin for 15 min before adding TGF-β significantly decreased the abundance of pSmad (Supplemental Figure S2, B and C) compared with DMSO controls and blocked nuclear translocation of Smad2 (Supplemental Figure S2D). These findings conflict with a recent report that the actin filament disrupting drugs cytochalasin and latrunculin do not inhibit increased pSmad2 in renal tubular epithelial cells treated with TGF-β (Muehlich *et al.*, 2017).

To determine how formin activity might be necessary for increased pSmad2 with TGF-β we first tested actomyosin contractility, which is increased by formin activity, and we found that in A549 cells pMLC increased with TGF-β in DMSO controls but not in the presence of SMHFH2 (Figure 1C). We treated A549 cells with Y-27632, which inhibits Rho-kinase activity, and with blebbistatin, which inhibits myosin II activity. Neither inhibitor blocked the increase in pSmad2 with TGF-β, the decrease in E-cadherin or the increase in Snail or fibronectin (with markedly more fibronectin with Y-27632 compared with DMSO controls) (Figure 4E). This lack of blocking increased pSmad2 was despite the efficacy of the inhibitors, which we confirmed. Y-27632 blocked the increase in pMLC (Figure 4E) and Y-27632 and blebbistatin both prevented the assembly of actin stress fibers with EMT (Figure 4F).

To further test a mechanism for formin-dependent pSmad, we next asked whether SMIFH2 alters the plasma membrane expression or dimerization of TGF-β receptors. TGF-β signaling is initiated by ligand binding to the type 2 receptor (TGF-βR2), which phosphorylates and dimerizes with the type 1 receptor (TGF-βR1). Kinase activity of TGF-βR1 phosphorylates Smad2 (Heldin and Moustakas, 2012). Accordingly, TGF-β signaling is dependent on the abundance of TGF-βR1 and TGF-βR2 at the plasma membrane as well as their dimerization and intracellular trafficking (Chen, 2009; Huang and Chen, 2012; Ganguly *et al.*, 2015). To test whether SMIFH2 affects the abundance of TGF-βR1 at the plasma membrane we biotinylated A549 cells stably expressing the receptor tagged with a Flag epitope, immunoprecipitated biotinylated proteins, and immunoblotted immune complexes with Flag antibodies. SMIFH2 had no effect on the abundance of TGF-βR1 in the absence of TGF-β or on the ligand-induced decrease in cell surface expression of TGF-βR1 seen with DMSO controls at 30 and 60 min (Figure 5A), suggesting that cell surface expression and the dynamics of TGF-βR1 are not dependent on formin activity. We also found that SMIFH2 had no observable effect on TGF-βR1 and TGF-βR2 dimerization with TGF-β. A549 cells transiently coexpressing TGF-βR1 tagged with a Myc epitope and TGF-βR2-Flag were treated with TGF-β and Flag immune complexes from

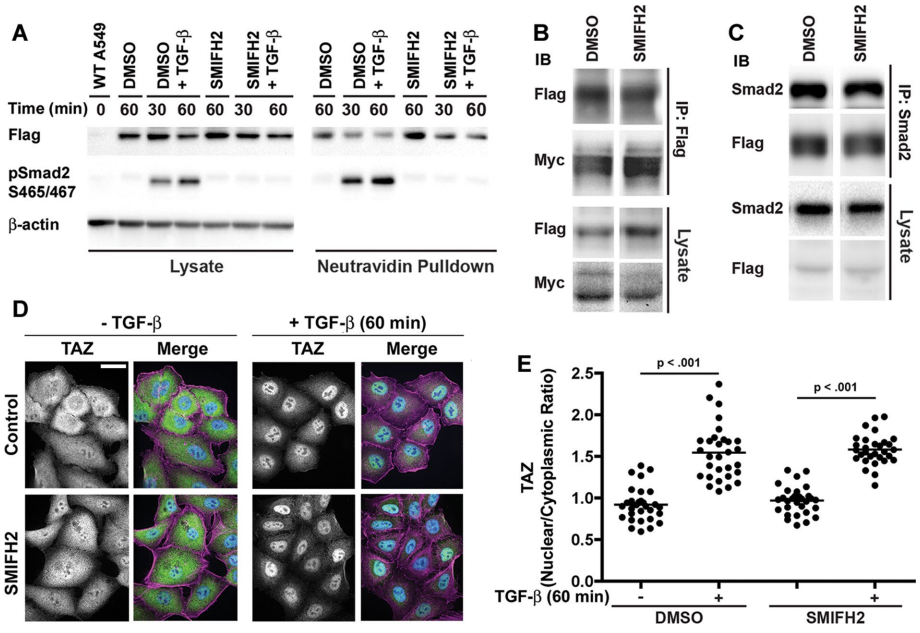

FIGURE 5: SMIFH2 does not decrease plasma membrane abundance or dimerization of TGF-β type 1 receptor or nuclear translocation of TAZ in A549 cells. (A) Cells stably expressing Flag-tagged TGF-β R1 were treated with TGF-β in the absence (DMSO) or presence of SMIFH2 for the indicated times. Cell surface expression of TGF-β R1-Flag was determined by immunoblotting neutravidin complexes from biotinylated cells. (B) Immunoblots with antibodies to Myc and Flag of total lysates and Flag immune complexes from cells transiently expressing TGF-β R1-Myc and TGF-β R2-Flag. Cells were treated with TGF-β for the indicated times in the absence (DMSO) or presence of SMIFH2 before lysis. (C) Immunoblots with antibodies to Flag and Smad2 of Smad2 immune complexes from cells stably expressing TGF-β R1-Flag and treated for 15 min with TGF-β in the absence (DMSO) or presence of SMIFH2. (D) Confocal images of cells maintained in the absence (–) or presence (+) of TGF-β for 60 min without (DMSO) or with SMIFH2 immunolabeled for TAZ (green) and costained with DAPI for nuclei (blue) and rhodamine–phalloidin for actin filaments (magenta). Bar, 20 μm. (E) Nuclear to cytoplasmic ratio of TAZ from immunolabeling as shown in C quantified for 30–35 cells per condition from two independent cell preparations.

cell lysates were immunoblotted with Myc antibodies. There was no difference in the abundance of coprecipitated TGF-βR1 in the absence or presence of SMIFH2 (Figure 5B). Additionally, SMIFH2 had no effect on the abundance of endogenous Smad2 coprecipitating with TGF-βR1-Flag stably expressed in A549 cells after TGF-β treatment (Figure 5C).

Consistent with SMIFH2 not blocking receptor membrane abundance or dimerization, we found that the inhibitor also did not block nuclear translocation of the Hippo signaling protein TAZ with TGF-β. TAZ and the Yes-associated protein YAP are transcriptional coactivators mediating effects of Hippo signaling for cell differentiation and tissue homeostasis. Although cross-talk between TGF-β signaling and TAZ/YAP is recognized, the precise regulatory mechanisms remain unresolved and are likely dependent on cell type and context (Hansen *et al.*, 2016). In A549 cells treated with TGF-β for 60 min, both DMSO control cells and cells treated with SMIFH2 had a significant increase in the TAZ nuclear to cytoplasmic ratio. In addition to further suggesting that SMIFH2 does not affect signaling at the level of the TGF-β receptor, these findings confirm that nuclear translocation of TAZ is independent of pSmad2 and also the specificity of SMIFH2 effects, which our data suggest are selective for TGF-β receptor activation of Smad2 but not for cross-talk with TAZ.

DIAPH1 and DIAPH3 are necessary for EMT with TGF-β

We next sought to identify the formin(s) necessary for TGF-β signaling and EMT, which would also validate formin-selective effects of SMIFH2. Nearly all of the 15 mammalian formins are expressed in epithelial cells of different tissue origins (Krainer *et al.*, 2013). We infected cells with lentivirus expressing formin-specific shRNA sequences and used nontargeting shRNA for controls. However, because antibodies to some formins are not available, we were limited to confirming suppressed expression of seven formins: DIAPH (1-3), DAAM1, FHOD1, FMNL1, and Formin1 (Supplemental Figure S3, A and B). Formin1 expression but not the expression of other formins decreased with 48 h of TGF-β treatment. In A549 cells, none of the individual formin shRNA we tested blocked increased pSmad2 or down-regulation of E-cadherin with TGF-β (Figure 6A and Supplemental Figure S3B). However, FHOD1 shRNA but not shRNA for other formins blocked the morphological program of changes in cell morphology and acquisition of actin stress fibers (Figure 6B), which is consistent with previous reports that FHOD1 is necessary for morphological transitions but not transcriptional events with EMT (Jurmeister *et al.*, 2012; Gardberg *et al.*, 2013). The specificity of FHOD1 shRNA blocking actin stress fiber assembly was confirmed by rescue with heterologously expressed full-length GFP-FHOD1 resistant to the shRNA (Supplemental Figure S3C).

In contrast with our finding with A549 cells, however, in HK2 cells shRNA for either DIAPH1 or DIAPH3 but not other formins significantly blocked the increase in pSmad, Snail, and N-cadherin with TGF-β compared with control NT cells (Figure 6, C–E). Respective shRNA sequences decreased expression of DIAPH1 and 2 (Figure 6C) and DIAPH 3 (Supplemental Figure S3D). Consistent with findings in A549 cells, FHOD1 shRNA did block increased pSmad2 (Supplemental Figure S3E). These data suggested the possibility of redundancy between DIAPH family formins in A549 cells, which we confirmed by using pooled shRNA to suppress formin family members in A549 cells. We confirmed specificity of DIAPH knockdown by immunoblotting with specific antibodies (Supplmental Figure S4A) and found that pooled shRNA targeting DIAPH1, 2, and 3 but not pooled shRNA for FMNL1 and 2 attenuated increased pSmad2 and Snail after 48 h with TGF-β (Figure 7, A–C), although these responses were not completely blocked as in HK2 cells. Compared with control NT shRNA, DIAPH1-3 pooled shRNA also attenuated the abundance of ventral actin stress fibers after 48 with TGF-β (Figure 7D), and actin filament abundance was in part rescued with heterologously expressed mouse GFP-DIAPH3 but not GFP alone, consistent with redundancy between DIAPH1 and 3 (Supplemental Figure S4). Additionally, in A549 cells, pooled shRNA for DIAPH1, 2, and 3 but not for DAMM 1 and 2 attenuated acute increases in pSmad2 with TGF-β between 10 and 60 min (Figure 7E). These data

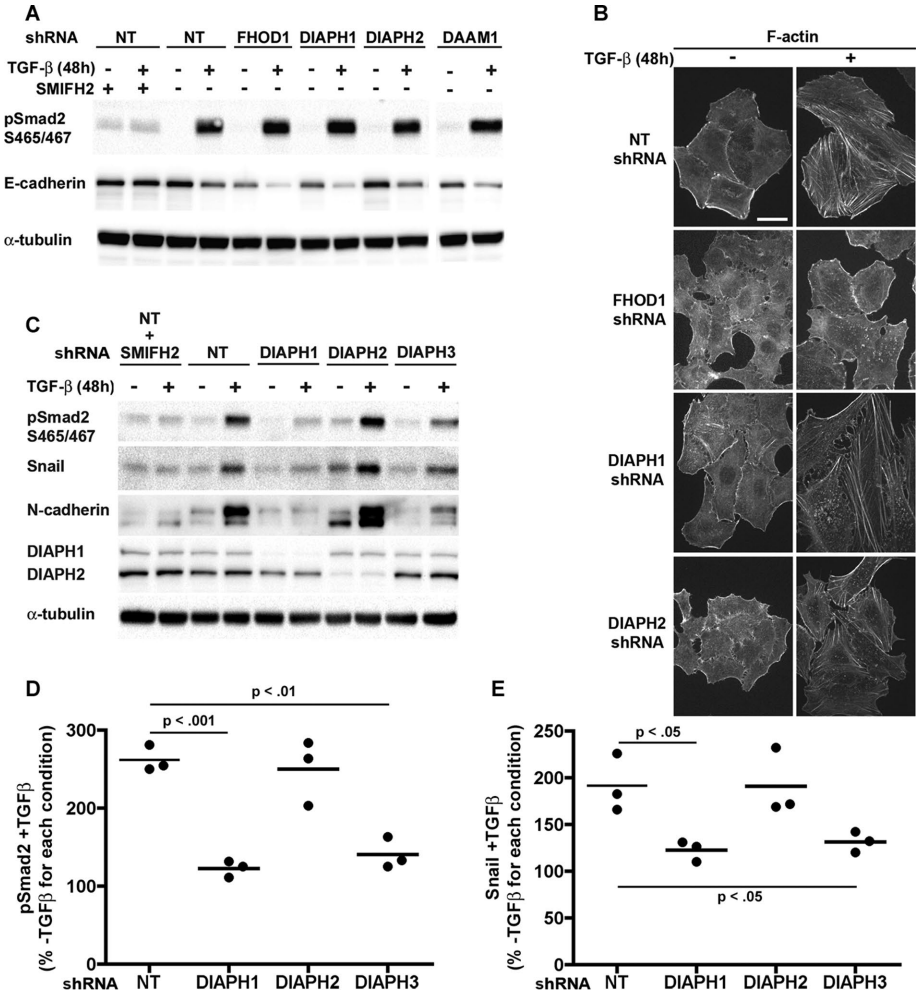

FIGURE 6: Formin-selective shRNA to test effects on EMT by TGF-β. (A) Immunoblots of lysates of A549 cells infected with lentivirus containing nontargeting (NT) or the indicated formin-selective shRNA, maintained in the absence (–) or presence (+) of TGF-β for 48 h and probed for pSmad2, E-cadherin, and α-tubulin. Blots are representative of two independent cell preparations. (B) Confocal images of A549 cells expressing the indicated formin shRNA and labeled for actin filaments with rhodamine–phalloidin. Images are representative of three independent cell preparations and show maximum-intensity projections of multiple Z-sections. Bar, 20 μm. (C) Immunoblots of lysates of HK2 cells infected with lentivirus containing NT or the indicated formin-selective shRNA, maintained in the absence (–) or presence (+) of TGF-β for 48 h and probed for pSmad2, Snail, N-cadherin, DIAPH1 and DIAPH 2, and α-tubulin.
(D, E) Semiquantitative densitometry of immunoblots described in C probed for pSmad (D) and Snail (E) obtained from three independent cell preparations.

indicate cell-specific effects of DIAPH family formins in TGF-β signaling, with DIAPH1 or DIAPH3 independently being necessary in HK2 cells but redundancy of these two formins in A549 cells.

DISCUSSION

Despite substantial remodeling of actin filaments and changes in cell shape during EMT, little is known about how this morphological program for EMT is regulated compared with the well-studied EMT transcription program (Xu *et al.*, 2009). One key finding of our study is that actin nucleation by formins but not the Arp2/3 complex is necessary for both morphological and transcription programs driving EMT in response to TGF-β, which we confirmed for three distinct epithelial cell types; human A549 lung alveolar and HK2 kidney epithelial cells and mouse NMuMG mammary epithelial cells. Inhibiting formin activity with the broad-spectrum formin inhibitor SMIFH2 (Rizvi *et al.*, 2009), but not Arp2/3 complex activity with the selective inhibitor CK666 (Nolen *et al.*, 2009), not only blocked a mesenchymal morphology and acquisition of actin stress fibers but also decreased expression of E-cadherin and increased expression of fibronectin and Snail. In contrast to our findings, WASP-interacting protein (WIP), a regulator of nuclear promoting factors activating the Arp2/3 complex, was reported to be necessary for the morphological program of EMT (Salvi and Thanabalu, 2017); however, WIP is not necessary for the transcriptional programs of deceased E-cadherin or increased N-cadherin, which we found are blocked by SMIFH2. Using shRNA to different formin family members, we determined that FHOD1 shRNA blocked a mesenchymal morphology and actin stress fibers with EMT of A549 cells but had no effect on the transcriptional programs for decreased E-cadherin or increased fibronectin and Snail. These data are consistent with previous findings showing that FHOD1 is necessary for a mesenchymal morphology and assembly of actin stress fibers but not down-regulation of E-cadherin with TGF-β–induced EMT of clonal MDA-MB-231 human breast cancer cells (Jurmeister *et al.*, 2012; Gardberg *et al.*, 2013). In contrast, we found that shRNA to DIAPH1 and DIAPH 3 blocked proximal TGF-β signaling at the level of pSmad and hence both morphological and transcriptional EMT programs.

Our second key finding with broad impact beyond EMT is that inhibiting formin activity blocks increased pSmad2 by TGF-β, a critical initial step in TGF-β signaling for reprogramming of gene expression. These findings are in contrast to a previous report that SMIFH2 does not block increased pSmad2 during human myofibroblast differentiation with TGF-β (Sandbo *et al.*, 2013). The formin FMNL2 was found to be necessary for efficient EMT of a metastatic line of SW480 clonal colon adenocarcinoma cells treated with TGF-β (Li *et al.*, 2010), with FMNL2 siRNA partially but not completely suppressing decreased expression of E-cadherin and increased phosphorylation of Smad3. However, this study found no effect on increased abundance of Snail, and FMLN2-dependent changes in actin filament remodeling and acute TGF-β signaling (<24 h) were not determined. Our data show that inhibiting formin activity with SMIFH2 blocks acute (10–60 min) and sustained (48 h) increases in pSmad2 and the nuclear translocation of Smad2 but has no effect on Smad2 expression, the cell surface expression and dimerization of TGF-β receptors, or the association of Smad2 with TGF-βR1. Moreover, we found that shRNA for formins DIAPH1 and DIAPH 3 phenocopied blocking increased pSmad2 and Snail that we found with SMIFH2. Additionally, we found that intact actin filament network, which we disrupted with latrunculin, is necessary for increased pSmad2 and nuclear translocation of Smad2 with TGF-β. Vasodilator-stimulated phosphoprotein

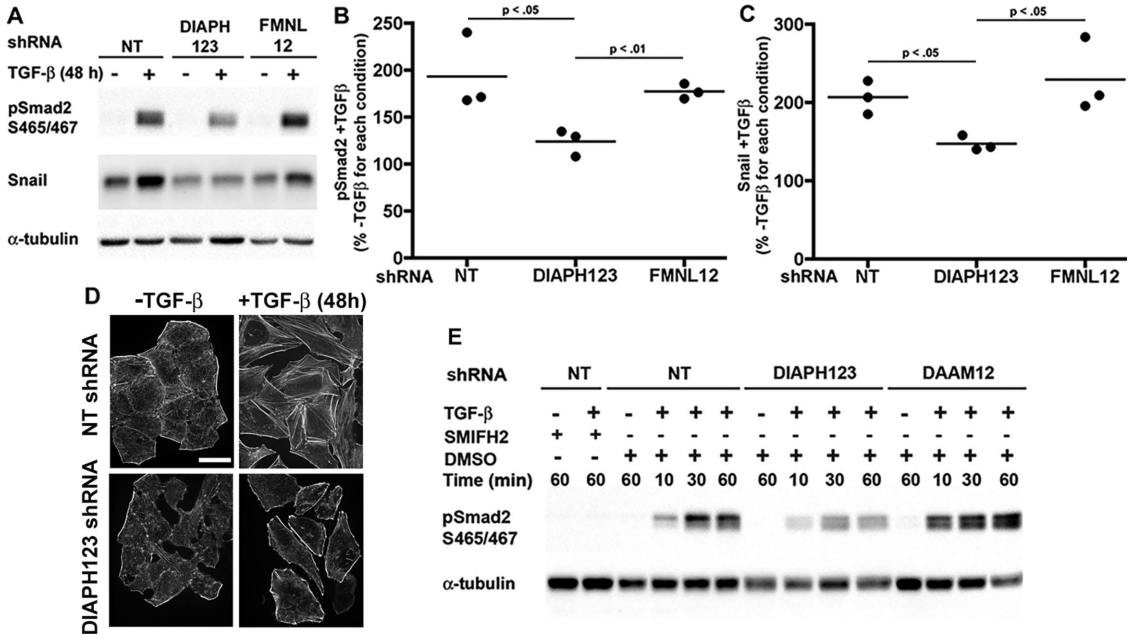

FIGURE 7: Pooled DIAPH123 shRNA inhibits TGF-β signaling in A549 cells. (A) Immunoblots of lysates from A549 cells infected with pooled formin shRNA and maintained in the in the absence (–) or presence (+) of TGF-β for 48 h probed for pSmad2 (S465/467), Snail, and α-tubulin. (B, C) Semiquantitative densitometry of immunoblots described in A for pSmad (B) and Snail (C) obtained from three independent cell preparations. (D) Images of A549 cells infected with lentivirus containing NT shRNA or DIAPH123 pooled shRNA and maintained in the absence (–) or presence (+) of TGF-β for 48 h stained for F-actin with rhodamine–phalloidin. Bar, 20 μm. (E) Representative immunoblots of two separate preparations of lysates from A549 cells expressing NT shRNA and pooled shRNA for DIAPH1, -2, and -3 and for DAAM1 and -2 and then treated with TGF-β for the indicated times and probed for pSmad2 (S465/467) and α-tubulin.

(VASP), a regulator of actin cytoskeleton remodeling, was recently shown to be necessary for targeting and maintaining TGF-βR2 to the plasma membrane (Tu *et al.*, 2015); however, our data with biotinylated cells showing no effect of SMIFH2 on the cell surface expression of TGF-βR1 suggest that this is not a mechanism for formin-dependent TGF-β signaling. Additionally, we predict that formins likely do not suppress negative regulation of TGF-β signaling by Smad7 (Shi *et al.*, 2004). Smad7 forms a stable complex with TGF-βR1 to inhibit Smad phosphorylation and receptor-Smad association; however, inhibiting formin activity had no effect on the abundance of Smad2 coprecipitating with TGF-βR1. Moreover, although SMIFH2 blocked increased pMLC with EMT, increased pSmad likely does not require formin-dependent actomyosin contractility because inhibiting contractility by blocking Rho-kinase or myosin II activity did not prevent increased pSmad with TGF-β.

Another important finding is that although inhibiting formin activity with SMIFH2 blocks increased pSmad2 and nuclear translocation of Smad2 with TGF-β, it does not block nuclear translocation of TAZ. These data confirm, first, that SMIFH2 does not block the fidelity of signaling by TGF-β receptors; second, the specificity of SMIFH2 for preventing increased pSmad; and, third, the recently reported finding that TGF-β regulation of TAZ is independent of Smads (Miranda *et al.*, 2017). One possibility for formin-dependent TGF-β signaling that is not currently feasible to experimentally test is whether actin filaments maintain a structural conformation of the TGF-βR1 necessary for increased pSmad2 but not for dimerizing with TGF-βR2 or activating TAZ.

Further investigation is warranted to determine how formin activity regulates pSmad2. One possibility is that formin-dependent actin architectures maintain a structural conformation of the TGF-βR1 necessary for kinase activity or for signal relay to Smad2 but not for TGF-βR1 and TGF-βR2 dimerization, the association of Smad2 with TGF-βR1, or the nuclear translocation of TAZ. An intriguing question that to our knowledge remains unanswered is whether TGF-β receptors are anchored to actin filaments, possibly through binding linker proteins such as the ERM family members ezrin, radixin, and moesin or through NHERF, as has been shown for receptor tyrosine kinases (Maudsley *et al.*, 2000; Karthikeyan *et al.*, 2002; Demoulin *et al.*, 2003) and G protein-coupled receptors (Hall *et al.*, 1998; Cao *et al.*, 1999; Li *et al.*, 2002; Heydorn *et al.*, 2004). Possible actin anchoring by TGF-β receptors is suggested by recent findings that the closely related type II bone morphogenic protein receptor scaffolds the actin cytoskeleton (Podkowa *et al.*, 2013). Another possibility is that formin-dependent actin architectures maintain TGF-β receptors in specialized membrane domains necessary for Smad2 phosphorylation. Consistent with this possibility, actin filaments regulate the organization and mobility of membrane proteins for downstream signaling (Mattila *et al.*, 2016) and TGF-β–induced Smad activation requires sequestration of receptors from caveolin-associated to clathrin-coated pits (Razani *et al.*, 2001; Penheiter *et al.*, 2002; Di Guglielmo *et al.*, 2003; Muthusamy *et al.*, 2015). Additionally, recent findings indicate that mechanical tension spatially segregates TGF-β receptors at the plasma membrane, with TGF-βR1 sequestered at integrin-rich focal adhesions but TGF-βR2 being excluded from these sites (Rys *et al.*, 2015). Hence, formin-dependent actin architectures could regulate differential partitioning of TGF-β receptor complexes at the cell surface.

Our findings indicate that DIAPH1 and DIAPH 3 are necessary for TGF-β signaling, with redundancy in A549 cells but not in HK2 cells. However, we cannot rule out an important role for additional formins in TGF-β signaling or EMT in other cell types. As discussed above, FMNL expression is necessary for TGF-β–induced EMT of clonal

metastatic colon adenocarcinoma cells, including the transcriptional program for decreased E-cadherin. Formins have been shown to regulate gene transcription, most notably by increasing activity of serum response factor (SRF) (Gasteier *et al.*, 2003; Westendorf and Koka, 2004; Xie *et al.*, 2008; Jurmeister *et al.*, 2012) or promoting nuclear translocation of myocardin-related transcription factor (MRTF), an SRF coactivator (Baarlink *et al.*, 2013). Moreover, nuclear translocation of MRTF is necessary for TGF-β–induced EMT (Korol *et al.*, 2016; O'Connor *et al.*, 2016) by regulating the morphological EMT program (O'Connor and Gomez, 2013)

Taken together, our findings on formin-dependent EMT have clinical significance for diseases such as cancer metastasis and fibrosis, which rely on epithelial transdifferentiation. And, importantly, our findings on formin-dependent TGF-β signaling have broad significance for understanding and for possible therapeutic insights on the myriad of normal and disease behaviors regulated by TGF-β.

MATERIALS AND METHODS

Cell culture and treatments

Clonal human lung A549 adenocarcinoma cells (obtained from Harold Chapman, University of California, San Francisco [UCSF]) were cultured in DMEM (4.5 g/l glucose) supplemented with 10% fetal bovine serum (FBS) (Invitrogen), 100 U/ml penicillin, and 100 µg/ml streptomycin as described previously (Haynes *et al.*, 2011; Rana *et al.*, 2015). For EMT, A549 cells were maintained in serum-free small airway basal medium (Lonza, Basel, Switzerland). Human HK2 cells (American Type Cell Collection) were maintained in DMEM with Hams F-12 containing 4.5 g/l glucose and supplemented with 10% FBS, 100 U/ml penicillin, and 100 µg/ml streptomycin. For EMT, HK2 cells were maintained in serum- and Ca^{2+}-free keratinocyte medium (Invitrogen) supplemented with 25 mg/ml bovine pituitary extract and 0.2 ng/ml epidermal growth factor (EGF), as described previously (Rana *et al.*, 2015). NMuMG normal mouse mammary gland epithelial cells (obtained from R. Derynck, UCSF) were maintained in DMEM containing 4.5 g/l glucose and supplemented with 10% FBS, 100 U/ml penicillin, 100 µg/ml streptomycin, and 10 µg/ml insulin (Sigma-Aldrich) as described previously (Haynes *et al.*, 2011). EMT was induced by adding recombinant TGF-β (PeproTech, Rocky Hill, NJ), using 10 ng/ml for HK2 cells and 5 ng/ml for A549 and NMuMG cells. Pharmacological inhibitors SMIFH2 (Sigma-Aldrich) and CK666 (Calbiochem) were dissolved in DMSO. Unless otherwise indicated, DMSO (control), SMIFH2 (25 µM), and CK666 (80 µM) were added at the time of TGF-β treatment and maintained in the medium for 48 h. 293FT cells used for generating lentivirus were maintained DMEM containing 4.5 g/l glucose and supplemented with 10% FBS, 100 U/ml penicillin, and 100 µg/ml streptomycin and NEAA. All cell lines were maintained at 37°C in 5% CO_2.

DNA constructs, lentivirus production, and transfections

For transient expression, A549 cells were transfected with pRK5 containing TGF-βR1-Myc (provided by Tamara Alliston, UCSF) or TGF-βR1-Flag (provided by R. Derynck, UCSF), pEGFP-C2 (Clonetech) containing full-length GFP-FHOD1 (provided by Stefan Linder, Universitätsklinikum Hamburg), or mEmerald-C1 containing mouse mDia3 (Addgene) using Lipofectamine 2000 (Invitrogen) according to the manufacturer's specifications. The lentiviral plasmids pLKO.1-puro containing shRNA sequences to human DIAPH1 (NM_005219; CCGGGCCCAGAATCTCTCAACTTTCTCGAGAAAGATTGAGAGATTCTGGGCTTTTT), DIAPH2 (NM_006729; CCGGCCTACAAAGAAGAAAGTGAAACTCGAGTTTCACTTTCTTCTTTGTAGGTTTTTG), DIAPH3 (NM_030932; CCGGCGTGTCAGAATAGCTAAAGAACTCGAGTTCTTTAGCTATTCTGACACGTTTTTTG), DAAM1 (NM_014992; CCGGGCACAATACTATCTCCTGAAACTCGAGTTTCAGGAGATAGTATTGTGCTTTTTG), DAAM2 (NM_015345; CCGGGCTCTTATTCAATACCACGTTCTCGAGAACGTGGTATTGAATAAGAGCTTTTTTG), FHOD1 (NM_013241; CCGGAGGTGCTGTATCCCGGAAATCCTCGAGGATTTCCGGGATACAGCACCTTTTTTG), FMNL2 (NM_052905; CCGGGCCAAGCAGAAGAACTCTGAACTCGAGTTCAGAGTTCTTCTGCTTGGCTTTTT), and Formin1 (NM_005892; CCGGATATTGGACTAGGATACAAATCTCGAGATTTGTATCCTAGTCCAATATTTTTTG) were obtained from Sigma-Aldrich (MISSION shRNA) as was MISSION Non-Target shRNA Control Vector. Lentivirus was produced in 293FT packaging cells using the Virapower Packaging System (Invitrogen) according to the manufacturer's protocol. A549 and HK2 cells were infected with lentivirus expressing control or formin shRNA in growth medium supplemented with 4 µg/ml Sequabrene (Sigma-Aldrich). Stable clonal cell lines were selected with 5 µg/ml puromycin (Cellgro; Mediatech, Manassas, VA) and maintained in 2.5 µg/ml puromycin. Retroviral plasmid LNCX TGF-βR1-Flag (obtained from Rik Derynck) was expressed in 293T Ampho cells with packaging plasmid PCL-Ampho for infection of A549 cells in growth medium supplemented with 4 µg/ml Sequabrene (Sigma-Aldrich). Stable A549 clones expressing TGF-βR1-Flag were selected and maintained in the antibiotic G418 (Life Technologies).

Immunolabeling, staining, and image acquisition

For immunolabeling, cells plated on acid-washed glass coverslips were washed at the indicated times in phosphate-buffered saline (PBS), fixed with 4% formaldehyde for 15 min, permeabilized with 0.2% Triton X-100 for 5 min, incubated with 5% horse serum and 1% bovine serum albumin (BSA) in PBS for 1 h, and then incubated with antibodies for E-cadherin (for A549 cells, 1:500, Invitrogen; for NMuMG cells, 1:200, BD Transduction Laboratories), Smad2 (1:200, Cell Signaling), or TAZ (1:200, Sigma) overnight at 4°C. The coverslips were washed with PBS and then incubated for 1 h at room temperature (RT) with Alexa-Fluor-488–conjugated secondary antibodies (Invitrogen). Actin filaments were labeled with rhodamine–phalloidin (1:500; Invitrogen) added during secondary antibody incubations. Nuclei were labeled with DAPI (1:10,000) added during the final wash after immunolabeling. Coverslips were mounted on slides with ProLong Gold antifade reagent (Invitrogen). Cells were imaged using a 60X Plan Apochromat TIRF 1.45 NA oil immersion objective on an inverted microscope system (Nikon Eclipse TE2000 Perfect Focus System; Nikon Instruments, Melville, NY) equipped with a spinning-disk confocal scanner unit (CSU10; Yokogawa, Newnan, GA), a 488-nm solid-state laser (LMM5; Spectral Applied Research), a multipoint stage (MS-2000; Applied Scientific Instruments), a CoolSnap HQ2 cooled charge-coupled camera (Photometrics,) and camera-triggered electronic shutters controlled with NIS-Elements Imaging Software (Nikon). Images were processed using NIS-Elements and rhodamine–phalloidin fluorescence was quantified using images processed using the ImageJ automated filter "Find Edges." Briefly, this algorithm uses a Sobel edge detection operator to highlight sharp changes in intensity using two 3×3 convolution kernels that generate vertical and horizontal derivatives of pixel values. The final processed image features enhanced edges produced by combining the two derivatives using the square root sum of the squares.

Immunoblotting, biotinylation, and Immunoprecipitation

For immunoblotting, cells were lysed in RIPA buffer (50 mM Tris-HCl, pH 7.5, 150 mM NaCl, 1 mM EDTA, 1 mM vanadate, 1 mM NaF,

1% Triton X-100, 0.1% deoxycholate, supplemented with protease inhibitor tablets). After centrifuging lysates at 12,000 rpm for 5 min to obtain a postnuclear supernatant, proteins were separated by SDS–PAGE and transferred onto polyvinylidene difluoride (PVDF) membranes (Millipore, Haywood, CA) as previously described (Haynes *et al.*, 2011; Rana *et al.*, 2015). Membranes were blocked with 5% nonfat milk or 5% BSA and incubated with primary antibodies for 1 h at RT or overnight at 4°C. Primary antibodies included fibronectin, Flag-M2, α-tubulin, FHOD1, and DIAPH2 (Sigma-Aldrich), pSmad2 (S465/467), Smad2, Snail, pMLC-Thr18/ Ser19 (Cell Signaling Technologies), E-cadherin (BD Transduction Labs), β-actin (Santa Cruz), and DIAPH1, DIAPH3, FMNL1, and DAAM1 (Proteintech Inc). After washing, membranes were incubated with horseradish peroxidase–conjugated secondary antibodies (Bio Rad Laboratories) for 1 h at room temperature and immunoreactivity visualized with enhanced femtochemiluminescence (Thermo Scientific) and imaged using a BioRad Chemidoc XRS. BioRad Chemidoc XRS Image Lab software was used for semiquantitative densitometric analysis of immunoblots. Prism software was used for plotting data and statistical analysis.

Variations of the above protocol included assays using biotinylation and immunoprecipitation. Cell surface expression of TβRI was determined by biotinylating cells and isolating cell surface biotinylated proteins using a commercially available kit (Pierce Cell Surface Protein Isolation kit; Thermo Fisher Scientific). A549 cells were biotinylated on ice for 30 min and lysed. Biotinylated proteins were isolated and probed by immunoblotting with antibodies to TβRI-Flag. For immunprecipitation, cell lysates were prepared in RIPA buffer as described for immunoblotting and then inclubated with anti-Flag-M2 magnetic beads (Sigma-Aldrich; cat. no. M8823) overnight at 4°C. The beads were washed three times and boiled in sample buffer for 5 min. Proteins in immune complexes were separated by SDS–PAGE for immunoblotting as described above.

Listeria monocytogenes motility in host cells

CCL39 fibroblasts stably expressing Lifeact-GFP were plated in MatTek dishes and incubated for 8–10 h with *L. monocytogenes* expressing mCherry-ActA (provided by Anna Bakardjiev, UCSF). Cells were washed 2× with PBS prior to time-lapse imaging using the microscopy unit described above for image acquisition. Velocity of moving *Listeria* was measured by using NIS-Elements Imaging Software by tracking displacement length as a function of time.

ACKNOWLEDGMENTS

We thank members of the Barber and Wittmann labs for constructive discussions. We thank Rik Derynck, Tamara Alliston, Hal Chapman, and Stefan Linder for providing reagents. We also thank B. P. Muthusamy and Koy Sateurn in the Derynck lab and David Monteiro in the Alliston lab for technical advice. This work was supported by National Institutes of Health grant GM116384 to D.L.B. and Todd Nystul.

REFERENCES

Baarlink C, Wang H, Grosse R (2013). Nuclear actin network assembly by formins regulates the SRF coactivator MAL. Science 340, 864–867.

Bhowmick NA, Ghiassi M, Bakin A, Aakre M, Lundquist CA, Engel ME, Arteaga CL, Moses HL (2001). Transforming growth factor-beta1 mediates epithelial to mesenchymal transdifferentiation through a RhoA-dependent mechanism. Mol Biol Cell 12, 27–36.

Borok Z, Whitsett JA, Bitterman PB, Thannickal VJ, Kotton DN, Reynolds SD, Krasnow MA, Bianchi DW, Morrisey EE, Hogan, BL, *et al* (2011). Cell plasticity in lung injury and repair: report from an NHLBI workshop. Proc Am Thorac Soc 8, 215–222.

Cao TT, Deacon HW, Reczek D, Bretscher A, von Zastrow M (1999). A kinase-regulated PDZ-domain interaction controls endocytic sorting of the beta2-adrenergic receptor. Nature 401, 286–290.

Chen YG (2009). Endocytic regulation of TGF-beta signaling. Cell Res 19, 58–70.

Cho HJ, Yoo J (2007). Rho activation is required for transforming growth factor-beta-induced epithelial-mesenchymal transition in lens epithelial cells. Cell Biol Int 31, 1225–1230.

Demoulin JB, Seo JK, Ekman S, Grapengiesser E, Hellman U, Ronnstrand L, Heldin CH (2003). Ligand-induced recruitment of Na+/H+-exchanger regulatory factor to the PDGF (platelet-derived growth factor) receptor regulates actin cytoskeleton reorganization by PDGF. Biochem J 376, 505–510.

Di Guglielmo GM, Le Roy C, Goodfellow AF, Wrana, JL (2003). Distinct endocytic pathways regulate TGF-beta receptor signalling and turnover. Nat Cell Biol 5, 410–421.

Ganguly A, Tang Y, Wang L, Ladt K, Loi J, Dargent B, Leterrier C, Roy S (2015). A dynamic formin-dependent deep F-actin network in axons. J Cell Biol 210, 401–417.

Gardberg M, Kaipio K, Lehtinen L, Mikkonen P, Heuser VD, Talvinen K, Iljin K, Kampf C, Uhlen M, Grenman R, *et al* (2013). FHOD1, a formin upregulated in epithelial-mesenchymal transition, participates in cancer cell migration and invasion. PLoS One 8, e74923.

Gasteier JE, Madrid R, Krautkramer E, Schroder S, Muranyi W, Benichou S, Fackler OT (2003). Activation of the Rac-binding partner FHOD1 induces actin stress fibers via a ROCK-dependent mechanism. J Biol Chem 278, 38902–38912.

Goley ED, Welch MD (2006). The ARP2/3 complex: an actin nucleator comes of age. Nature reviews. Mol Cell Biol 7, 713–726.

Goode BL, Eck MJ (2007). Mechanism and function of formins in the control of actin assembly. Ann Rev Biochem 76, 593–627.

Hall RA, Ostedgaard LS, Premont RT, Blitzer JT, Rahman N, Welsh MJ, Lefkowitz, RJ (1998). A C-terminal motif found in the beta2-adrenergic receptor, P2Y1 receptor and cystic fibrosis transmembrane conductance regulator determines binding to the Na+/H+ exchanger regulatory factor family of PDZ proteins. Proc Natl Acad Sci USA 95, 8496–8501.

Hansen CG, Moroishi T, Guan KL (2016) YAP and TAZ: a nexus for Hippo signaling and beyond. Trends Cell Biol 25, 499–513.

Haynes J, Srivastava J, Madson N, Wittmann T, Barber DL (2011). Dynamic actin remodeling during epithelial-mesenchymal transition depends on increased moesin expression. Mol Biol Cell 22, 4750–4764.

Heldin CH, Moustakas A (2012). Role of Smads in TGFbeta signaling. Cell Tissue Res 347, 21–36.

Heydorn A, Sondergaard BP, Ersboll B, Holst B, Nielsen FC, Haft CR, Whistler J, Schwartz TW (2004). A library of 7TM receptor C-terminal tails. Interactions with the proposed post-endocytic sorting proteins ERM-binding phosphoprotein 50 (EBP50), N-ethylmaleimide-sensitive factor (NSF), sorting nexin 1 (SNX1), and G protein-coupled receptor-associated sorting protein (GASP). J Biol Chem 279, 54291–54303.

Huang F, Chen YG (2012). Regulation of TGF-beta receptor activity. Cell Biosci 2, 9–19.

Jeon YJ, Jung N, Park JW, Park HY, Jung, SC (2015). Epithelial-mesenchymal transition in kidney tubular epithelial cells induced by globotriaosylsphingosine and globotriaosylceramide. PLoS One 10, e0136442.

Jurmeister S, Baumann M, Balwierz A, Keklikoglou I, Ward A, Uhlmann S, Zhang JD, Wiemann S, Sahin O (2012). MicroRNA-200c represses migration and invasion of breast cancer cells by targeting actin-regulatory proteins FHOD1 and PPM1F. Mol Cell Biol 32, 633–651.

Kalluri R, Neilson EG (2003). Epithelial-mesenchymal transition and its implications for fibrosis. J Clin Invest 112, 1776–1784.

Kalluri R, Weinberg RA (2009). The basics of epithelial-mesenchymal transition. J Clin Invest 119,1420–1428.

Karthikeyan S, Leung T, Ladias JA (2002). Structural determinants of the Na+/H+ exchanger regulatory factor interaction with the beta 2 adrenergic and platelet-derived growth factor receptors. J Biol Chem 277,18973–18978.

Korol A, Taiyab A, West-Mays JA (2016). RhoA/ROCK signaling regulates TGFbeta-induced epithelial-mesenchymal transition of lens epithelial cells through MRTF-A. Mol Med 22, 713–723.

Krainer E., Ouderkirk JL, Miller EW, Miller MR, Mersich AT, Blystone SD (2013). The multiplicity of human formins: expression patterns in cells and tissues. Cytoskeleton 70, 424–38.

Lamouille S, Derynck R (2007). Cell size and invasion in TGF-beta-induced epithelial to mesenchymal transition is regulated by activation of the mTOR pathway. J Cell Biol 178, 437–451.

Lamouille S, Xu J, Derynck R (2014). Molecular mechanisms of epithelial-mesenchymal transition. Nat Rev Mol Cell Biol 15, 178–196.
Li JG, Chen C, Liu-Chen LY (2002). Ezrin-radixin-moesin-binding phosphoprotein-50/Na+/H+ exchanger regulatory factor (EBP50/NHERF) blocks U50,488H-induced down-regulation of the human kappa opioid receptor by enhancing its recycling rate. J Biol Chem 277, 27545–27552.
Li Y, Zhu X, Zeng Y, Wang J, Zhang X, Ding YQ, Liang L (2010). FMNL2 enhances invasion of colorectal carcinoma by inducing epithelial-mesenchymal transition. Mol Cancer Res 8, 1579–1590.
Mattila PK, Batista FD, Treanor B (2016). Dynamics of the actin cytoskeleton mediates receptor cross talk: an emerging concept in tuning receptor signaling. J Cell Biol 212, 267–280.
Maudsley S, Zamah AM, Rahman N, Blitzer JT, Luttrell LM, Lefkowitz RJ, Hall RA (2000). Platelet-derived growth factor receptor association with Na(+)/H(+) exchanger regulatory factor potentiates receptor activity. Mol Cell Biol 20, 8352–8363.
May RC, Hall ME, Higgs HN, Pollard TD, Chakraborty T, Wehland J, Machesky LM, Sechi AS (1999). The Arp2/3 complex is essential for the actin-based motility of Listeria monocytogenes. Curr Biol 9, 759–762.
Miettinen PJ, Ebner R, Lopez AR, Derynck R (1994). TGF-beta induced transdifferentiation of mammary epithelial cells to mesenchymal cells: involvement of type I receptors. J Cell Biol 127, 2021–2036.
Miranda MZ, Bialik JF, Speight P, Dan Q, Yeung T, Szászi K, Pedersen SF, Kapus A (2017) TGF-β1 regulates the expression and transcriptional activity of TAZ protein via a Smad3-independent, myocardin-related transcription factor-mediated mechanism. J Biol Chem 292, 14902–14920.
Mori M, Nakagami H, Koibuchi N, Miura K, Takami Y, Koriyama H, Hayashi H, Sabe H, Mochizuki N, Morishita R, Kaneda Y (2009). Zyxin mediates actin fiber reorganization in epithelial-mesenchymal transition and contributes to endocardial morphogenesis. Mol Biol Cell 20, 3115–3124.
Muehlich S, Rehm M, Ebenau A, Goppelt-Struebe M (2017) Synergistic induction of CTGF by cytochalasin D and TGFβ-1 in primary human renal epithelial cells: role of transcriptional regulators MKL1, YAP/TAZ and Smad2/3. Cell Signal 29, 31–4.
Muthusamy BP, Budi EH, Katsuno Y, Lee MK, Smith SM, Mirza AM, Akhurst RJ, Derynck R. (2015). ShcA protects against epithelial-mesenchymal transition through compartmentalized inhibition of TGF-beta-induced Smad activation. PLoS Biol 13, e1002325.
Nolen BJ, Tomasevic N, Russell A, Pierce DW, Jia Z, McCormick CD, Hartman J, Sakowicz R, Pollard TD (2009). Characterization of two classes of small molecule inhibitors of Arp2/3 complex. Nature 460, 1031–1034.
O'Connor JW, Gomez EW (2013). Cell adhesion and shape regulate TGF-beta1-induced epithelial-myofibroblast transition via MRTF-A signaling. PLoS One 8, e83188.
O'Connor JW, Mistry K, Detweiler D, Wang C, Gomez EW (2016). Cell-cell contact and matrix adhesion promote alphaSMA expression during TGFbeta1-induced epithelial-myofibroblast transition via Notch and MRTF-A. Sci Rep 6, 26226.
Penheiter SG, Mitchell H, Garamszegi N, Edens M, Dore JJ Jr, Leof EB (2002). Internalization-dependent and -independent requirements for transforming growth factor beta receptor signaling via the Smad pathway. Mol Cell Biol 22, 4750–4759.
Podkowa M, Christova T, Zhao X, Jian Y, Attisano L (2013). p21-Activated kinase (PAK) is required for bone morphogenetic protein (BMP)-induced dendritogenesis in cortical neurons. Mol Cell Neurosci 57, 83–92.
Rana MK, Srivastava J, Yang M, Chen CS, Barber DL (2015). Hypoxia increases the abundance but not the assembly of extracellular fibronectin during epithelial cell transdifferentiation. J Cell Sci 128, 1083–1089.
Razani B, Zhang XL, Bitzer M, von Gersdorff G, Bottinger EP, Lisanti MP (2001). Caveolin-1 regulates transforming growth factor (TGF)-beta/SMAD signaling through an interaction with the TGF-beta type I receptor. J Biol Chem 276, 6727–6738.
Rizvi SA, Neidt EM, Cui J, Feiger Z, Skau CT, Gardel ML, Kozmin SA, Kovar DR (2009). Identification and characterization of a small molecule inhibitor of formin-mediated actin assembly. Chem Biol 16, 1158–1168.
Rys JP, DuFort CC, Monteiro DA, Baird MA, Oses-Prieto JA, Chand S, Burlingame AL, Davidson MW, Alliston TN (2015). Discrete spatial organization of TGFβ receptors couples receptor multimerization and signaling to cellular tension. Elife 4, e09300.
Salvi A, Thanabalu T (2017) WIP promotes in-vitro invasion ability, anchorage independent growth and EMT progression of A549 lung adenocarcinoma cells by regulating RhoA levels. Biochem Biophys Res Commun 482, 1353–1359.
Sandbo N, Ngam C, Torr E, Kregel S, Kach J, Dulin N (2013) Control of myofibroblast differentiation by microtubule dynamics through a regulated localization of mDia2. J Biol Chem 288, 15466–15473.
Schonichen A, Geyer M (2010). Fifteen formins for an actin filament: a molecular view on the regulation of human formins. Biochim Biophys Acta 1803, 152–163.
Shi W, Sun C, He B, Xiong W, Shi X, Yao D, Cao X. (2004). GADD34-PP1c recruited by Smad7 dephosphorylates TGFbeta type I receptor. J Cell Biol 164, 291–300.
Tavares AL, Mercado-Pimentel ME, Runyan RB, Kitten GT (2006). TGF beta-mediated RhoA expression is necessary for epithelial-mesenchymal transition in the embryonic chick heart. Develop Dynam 235, 1589–1598.
Tu K, Li J, Verma VK, Liu C, Billadeau DD, Lamprecht G, Xiang X, Guo L, Dhanasekaran R, Roberts LR, *et al* (2015). Vasodilator-stimulated phosphoprotein promotes activation of hepatic stellate cells by regulating Rab11-dependent plasma membrane targeting of transforming growth factor beta receptors. Hepatology 61, 361–374.
Welch MD, Iwamatsu A, Mitchison TJ (1997). Actin polymerization is induced by Arp2/3 protein complex at the surface of Listeria monocytogenes. Nature 385, 265–269.
Westendorf JJ, Koka S (2004). Identification of FHOD1-binding proteins and mechanisms of FHOD1-regulated actin dynamics. J Cell Biochem 92, 29–41.
Xi Y, Tan K, Brumwell AN, Chen SC, Kim YH, Kim TJ, Wei Y, Chapman HA (2014). Inhibition of epithelial-to-mesenchymal transition and pulmonary fibrosis by methacycline. Am J Respir Cell Mol Biol 50, 51–60.
Xie Y, Tan EJ, Wee S, Manser E, Lim L, Koh CG (2008). Functional interactions between phosphatase POPX2 and mDia modulate RhoA pathways. J Cell Sci 121, 514–521.
Xu J, Lamouille S, Derynck R (2009). TGF-beta-induced epithelial to mesenchymal transition. Cell Res 19, 156–172.
Yang Q, Zhang XF, Pollard TD, Forscher P (2012). Arp2/3 complex-dependent actin networks constrain myosin II function in driving retrograde actin flow. J Cell Biol 197, 939–956.